RSC Advances

PAPER

View Article Online
View Journal | View Issue

Cite this: *RSC Adv.*, 2022, **12**, 29569

Exploring the adsorption ability with sensitivity and reactivity of C_{12}–B_6N_6, C_{12}–Al_6N_6, and B_6N_6–Al_6N_6 heteronanocages towards the cisplatin drug: a DFT, AIM, and COSMO analysis†

Md. Golam Muktadir, Ariful Alam, Afiya Akter Piya and Siraj Ud Daula Shamim *

The DFT study on the adsorption behaviour of the C_{24}, $B_{12}N_{12}$, and $Al_{12}N_{12}$ nanocages and their heteronanocages towards the anticancer drug cisplatin (CP) was performed in gas and water media. Among the three pristine nanocages, $Al_{12}N_{12}$ exhibited high adsorption energy ranging from −1.98 to −1.63 eV in the gas phase and −1.47 to −1.39 eV in water media. However, their heterostructures C_{12}–Al_6N_6 and B_6N_6–Al_6N_6 showed higher interaction energies (−2.22 eV and −2.14 eV for C_{12}–Al_6N_6 and B_6N_6–Al_6N_6) with a significant amount of charge transfer. Noteworthy variations in electronic properties were confirmed by FMO analysis and DOS spectra analysis after the adsorption of the cisplatin drug on $B_{12}N_{12}$ and B_6N_6–Al_6N_6 nanocages. Furthermore, an analysis of quantum molecular descriptors unveiled salient decrement in global hardness and increments in electrophilicity index and global softness occurred after the adsorption of CP on $B_{12}N_{12}$ and B_6N_6–Al_6N_6. On the other hand, the above-mentioned fluctuations are not so noteworthy in the case of the adsorption of CP on $Al_{12}N_{12}$, C_{12}–B_6N_6, and C_{12}–Al_6N_6. Concededly, energy calculation, FMO analysis, ESP map, DOS spectra, quantum molecular descriptors, dipole moment, COSMO surface analysis, QTAIM analysis, and work function analysis predict that $B_{12}N_{12}$ and B_6N_6–Al_6N_6 nanocages exhibit high sensitivity towards CP drug molecules.

Received 29th June 2022
Accepted 24th September 2022

DOI: 10.1039/d2ra04011e

rsc.li/rsc-advances

1. Introduction

Cancer is the leading contributor to the ailment burden across the globe, and studies predict that the global cancer burden will continue to grow for the forthcoming 20 years. Chemotherapy is a sheet anchor for cancer treatment along with surgical intervention and radiotherapy. However, it is a matter of fact that chemotherapeutic drugs inevitably attack normal cells along with proliferating cancerous cells, causing adverse effects. The adverse side effects include loss of immunity to other diseases, fall in appetite, nausea, loss of hair, *etc.* For this reason, advanced chemotherapeutics, which are capable of targeting cancerous cells (either actively or passively) and thereby omitting the adverse side effects, is a crying need. To guide and unload a drug at a specific predestined biological site in an efficient and controlled targeted drug delivery system may provide the best solution.

In 1844 M. Peyrone first synthesized cisplatin[1] and in 1965 Rosenberg elucidated the anticancer activity of cisplatin following the growth of bacteria under the influence of electrolysis products from platinum-based electrodes.[2,3] Clinically proven reports undoubtedly support cisplatin to combat different types of cancers, including lung cancer, sarcomas, ovarian cancer, carcinoma, breast cancer, and brain cancer.[1,4,5] However the therapeutic application of cisplatin is hindered by numerous (approximately 40 types) toxicities associated with it, including gastrointestinal toxicity, nephrotoxicity, cardiotoxicity followed by low specificity and poor solubility.[6–8] A high-resolution crystallographic study conducted by Nicolla Pontillo *et al.* concluded that ferritin nanocages can be prominent cisplatin delivery platforms to minimize the off-target toxicity.[9] In addition to this, numerous DFT approaches have been performed to reduce the side effects of cisplatin and enhance the therapeutic outcomes.[5,10–12] For this reason, we are enthusiastic to explore the adsorption ability of cisplatin drug on C_{24} and its derivative nanocages for the first time.

Nanomaterial-based delivery systems are making a noteworthy difference in cancer immunotherapy because of their unique biological characteristics. Owing to their large surface area to volume ratio, tiny size, binding or adsorption, and carrying anticancer agents with them is really feasible. Among different nanostructures, including nanodots, nanosheets, nanocage, nanowires, nanocones, and nanotubes, nanocages owing to their unique spherical shape, lesser adverse side effects, and enhanced sensitivity to drug molecules, have

Department of Physics, Mawlana Bhashani Science and Technology University, Tangail, Bangladesh. E-mail: sdshamim@mbstu.ac.bd

† Electronic supplementary information (ESI) available. See https://doi.org/10.1039/d2ra04011e

extensively drawn the attention of researchers.[13–15] Due to the good thermodynamic stability of C_{24} fullerene, numerous investigations have been conducted by considering C_{24} as an adsorbent.[16–18] Bodgan *et al.* have studied the adsorption behaviour of the ephedrine drug on C_{24} using DFT and TD-DFT theory and they have proposed C_{24} to be a potential carrier.[16] According to the investigation of Hosseinian *et al.*, the interaction between 5-fluorouracil and C_{24} fullerene was found to be a weak interaction, which was later enhanced by substituting one carbon atom with a boron atom.[17] To improve the interaction behaviour of C_{24}, its derivatives such as $B_{12}N_{12}$ and $Al_{12}N_{12}$ were widely studied by Javan *et al.* who theoretically proposed that $B_{12}N_{12}$ could be a favourable drug carrier for 5-fluorouracil drug by DFT.[19] Soltani *et al.* investigated the interaction of 5-AVA drug molecules on $B_{12}N_{12}$ and $B_{16}N_{16}$ nano-cages and concluded that $B_{12}N_{12}$ is more preferable for the drug than $B_{16}N_{16}$.[20] Using DFT computations, Fatemeh Azarakhshi *et al.* investigated the adsorption behaviour of sulfanilamide drugs on $B_{12}N_{12}$ and $Al_{12}N_{12}$. Afterward, they concluded that $B_{12}N_{12}$ fullerene can be suitable for the delivery of SLF drug.[21] Padash *et al.* studied the adsorption of sulfamide drugs employing DFT onto the exterior surface of $Al_{12}N_{12}$, $Al_{12}P_{12}$, $B_{12}N_{12}$, and $B_{12}P_{12}$ and concluded that $Al_{12}N_{12}$ showed the best adsorbent property.[22] Recently, different heteronanocages have been studied and proposed as drug delivery systems due to their unique properties, such as high interaction behaviour with drug molecules.[23–25] Muz *et al.* studied $C_{30}B_{15}N_{15}$ heteronanocages as a drug carrier for flavipiravir and Hazrati *et al.* investigated the same heteronanocages as isoniazid drug vehicles by DFT.[24,26] C_{12}–B_6N_6 and C_{12}–Al_6N_6 heteronanocages have been studied by X. F. Fan *et al.* and Paul *et al.* by theoretical studies and confirmed to be energetically stable.[25,27]

This study is aimed to set forth the adsorption ability of the C_{24} fullerene and its derivatives (substituting the C atoms with B, Al, and N atoms in equal proportions) for the controlled delivery of Cisplatin. Firstly, we investigated the sensitivity of C_{24} towards CP and found a weak interaction. Secondly, C_{24} nanocages were modified by substituting 12 C atoms with equal proportions of B, N, and Al atoms to enhance the adsorption characteristics. In order to further explore the bio-sensing of CP, we further modified the C_{24} nanocage and modelled fullerene-like heteronanocages, *i.e.* C_{12}–B_6N_6, C_{12}–Al_6N_6, and B_6N_6–Al_6N_6, and performed adsorption computations under DFT framework. To investigate the reactivity of our proposed nanocages towards CP, quantum molecular descriptors and work function analysis along with the quantum theory of atoms in molecules (QTAIM) and COSMO surface analysis were performed.

2. Computational details

This presented investigation under spin unrestricted DFT framework conditions illustrates the adsorption calculations of cisplatin over $Al_{12}N_{12}$, $B_{12}N_{12}$, C_{24}, C_{12}–B_6N_6, C_{12}–Al_6N_6, and B_6N_6–Al_6N_6 nanocages in gas and water phases implemented in $Dmol^3$ module.[28,29] In order to optimize the structures of the nanocages along with the complexes of cisplatin, generalized gradient approximation (GGA) (instead of LDA) was used, since local density approximation (LDA) estimates inflated results as observed in numerous previous studies for results of equilibrium distance and bond energy. To describe the exchange–correlation interaction, the Perdew–Burke–Ernzerhof (PBE) functional within GGA was used.[30,31] For the core treatment, DFT semi-core pseudopotentials along with double numerical basis set plus polarization (DNP) was applied in the absence of any symmetry restriction. The geometries have been optimized under spin unrestricted condition.[32] In order to account for the van der Waals interaction, all the investigations were carried out by implementing Tkatchenko–Scheffler (TS) dispersion corrected PBE, which also accounts for the long-range electron effect.[33] To account for the dispersion forces in the interactions precisely, the dispersion corrected DFT (DFT-D) scheme was adopted.[34] It is irrefutable that computations are prone to be affected by BSSE (basis set superposition error) if interacting molecules are present. Therefore, BSSE (basis set superposition error) correction is one of the important factors for obtaining precise energy of the complexes, and in this case, the DNP basis set has better accuracy since it can offset the effects of BSSE errors. In this study, the maximum displacement, maximum force, and convergence tolerance of energy were 0.005 Å, 0.004 Ha $Å^{-1}$, and 2×10^{-5} Ha, respectively.[35] The convergence of the electronic SCF was set to 1×10^{-5} eV. A 0.005 Ha smearing point and a 5 Å real space global cut-off radius for better computational accuracy and speedy geometry optimization were set.[36] Adsorption is defined as a surface phenomenon in which the adsorbate species from the solution accumulate on the solid adsorbent surface by van der Waals interaction, and it is mainly a consequence of the surface energy. The energy (E_{ad}) of cisplatin to get adsorbed on the surface of $Al_{12}N_{12}$, $B_{12}N_{12}$, and C_{24} nanocages is defined as follows:[37]

$$E_{ad} = E_{com} - E_{drug} - E_{cage} \quad (1)$$

In the above equation E_{com}, E_{drug}, E_{cage} denote the total energies of complexes, cisplatin drug, and nanocages, respectively. The electronic properties are well described by E_L (energy of the lowest unoccupied molecular orbital (LUMO)) and E_H (energy of the highest occupied molecular orbital (HOMO)) and the energy gap E_g fluctuations and relation among these mentioned parameters are as follows:

$$E_g = E_L - E_H \quad (2)$$

The change in the energy gap (% ΔE_g) of E_g is obtained as follows:

$$\% \Delta E_g = \left[\frac{E_{g2} - E_{g1}}{E_{g1}}\right] \times 100 \quad (3)$$

where E_{g2} and E_{g1} are the subsequent and initial values of energy gap E_g of nanocages after and before the adsorption of the mentioned drug, respectively. The quantum chemical descriptors,[38–41] were calculated using the following equations:

$$\text{Electrophilicity, } \omega = \mu^2/2\eta \quad (4)$$

$$\text{Softness, } S = 1/2\eta \quad (5)$$

$$\text{Hardness, } \eta = (E_{LUMO} - E_{HOMO})/2 \quad (6)$$

$$\text{Chemical potential, } \mu = -(E_{HOMO} + E_{LUMO})/2 \quad (7)$$

The analysis of the normal mode of vibrations was performed in order to ascertain that the structures after adsorption belongs to real local minima. The charge transfer among drug and nanocages were studied based on the Hirshfeld charge analysis. It analyses the electron density as a function of space, to know whether cisplatin acts as a donor or acceptor.[42] In a water solvent, the interaction of cisplatin drug with the nanocages was investigated by applying a dielectric constant of 78.54 by introducing the conductor-like screening model (COSMO).[43] To gain a further better revelation about the characteristics of the interactions, QTAIM analysis was performed on the considered complexes.[44,45] In this investigation, all parameters mentioned earlier were computed and all states were optimized once again in water media using the same theories.

3. Results and discussion

3.1. Geometry optimization

The nanocages we were interested (C_{24}, $Al_{12}N_{12}$, $B_{12}N_{12}$, C_{12}–B_6N_6, C_{12}–Al_6N_6, and B_6N_6–Al_6N_6 for drug delivery) were relaxed both in gas and water media. The optimized illustrations of the adsorbent nanocages are depicted in Fig. 1. The C_{24} nanocage consists of six 4-component rings (4-CR) attached to eight 6-component rings (6-CR) with $m\bar{3}m$ (O_h) symmetry and contains no 5-component ring (5-CR). In 4-CR, C–C bond lengths are equal and have been computed at about 1.490 Å, and in 6-CR, C–C bond lengths are also equal and have been computed at about 1.38 Å. Hence, the average C–C length in C_{24} nanocage is 1.435 Å, which is consistent with the previous studies by Chang *et al.* and Soliman *et al.*[46,47] In order to study the electron-rich and deficient regions, the HOMO and LUMO maps of the nanocages were analysed. For C_{24}, except for some of the C–C bonds in 4-CR and 6-CR, 6-CR, and 6-CR junctions, the HOMO and LUMO levels were located throughout the entire cage. In the case of $B_{12}N_{12}$ and $Al_{12}N_{12}$, the HOMO levels were above the N atoms and LUMO levels were situated over the B and Al atoms of the nanocages. Based on the results of the simulation, the energy gaps (E_g) were computed at about 1.577 eV, 4.972 eV, and 2.644 eV for C_{24}, $B_{12}N_{12}$, and $Al_{12}N_{12}$, respectively. The calculated E_g of C_{24} (1.577 eV) is consistent with the result obtained by Kosar *et al.* employing the B3LYP hybrid functional (1.81 eV).[48] The E_g of $B_{12}N_{12}$ was in good agreement with the result (4.43 eV) obtained employing B3LYP/6-31G(d,p) by Rakib Hossain *et al.* and mass spectrometric analysis by Oku *et al.*[49,50]

Increased electronegativity difference leads to an increased ionic character as well as increased bond polarity. The electronegativity values of boron (B), nitrogen (N), and aluminium (Al) were 2.051, 3.066, and 1.613, respectively. According to this, the difference in the electronegativity of N and B in $B_{12}N_{12}$ is 1. For $Al_{12}N_{12}$, the difference in electronegativity of the constituent molecules was 1.43, which is greater than the electronegativity difference of $B_{12}N_{12}$. Therefore, $Al_{12}N_{12}$ shows enhanced ionic character than $B_{12}N_{12}$. As $B_{12}N_{12}$ exhibits covalent character, its HOMO–LUMO gap (E_g) is greater than $Al_{12}N_{12}$.[51] The CP drug molecule was optimized and the relaxed structure along with its respective HOMO–LUMO profile and ESP map are depicted in Fig. SI1.† Previous experimental results agree with our observation on the bond lengths of the optimized CP drug.[52] Two kinds of N–H bonds have been perceived in CP having lengths of 1.035 Å and 1.023 Å. The Pt–N and Pt–Cl bond lengths were found to be 2.110 Å and 2.315 Å, respectively. While experimental values of these bonds were 2.06 Å and 2.347 Å; in fact, previous studies suggested the theoretically observed values of these bonds as 2.09 Å and 2.307 Å, respectively. The HOMO profile of the CP drug suggests that the HOMO levels are located on the Pt and Cl atoms at −5.029 eV. The LUMO profile shows that the LUMO level is located on the Pt–Cl and Pt–N bonds and H atoms at 2.36 eV. The accumulation of negative and positive charges around Cl atoms and the NH_3 molecules, respectively, was confirmed from the ESP map of CP.

3.2. Adsorption of CP on C_{24} nanocage

In search for suitable adsorbents for the CP drug, ample adsorption parameters of CP/C_{24}, CP/$B_{12}N_{12}$, and CP/$Al_{12}N_{12}$ complexes were investigated. Initially, on different adsorption domains of C_{24} nanocage, CP was adsorbed (both in gas and water media) and among them, four different orientations of the CP drug over C_{24} were chosen. The description of the states are as follows: (i) the S_1 state where CP was placed parallel to the C_{24} nanocage, (ii) the S_2 state where CP was placed perpendicular to the C_{24} nanocage and one Cl atom of the CP drug was close to the nanocage, (iii) the S_3 state where central Pt atom of the drug molecule was slightly far for the central top C atom of C_{24} than the S_1 and the drug was parallel to the nanocage, (iv) the S_4 state where two NH_3 of the CP were close to the central top C atom and the drug molecule was slightly inclined outwards from the nanocage perpendicularly. In the case of the complex molecules, the geometry of C_{24} was found unchanged and the bond lengths around the 4-CR and 6-CR junctions and 6-CR–6CR junctions were observed to vary about 0.044 Å and 0.046 Å, respectively. The optimized geometries, as well as the adsorption distances of all states (in the gas phase), were demonstrated in Fig. 2. Negative adsorption energies were observed for all the states, which indicates attractive interactions between the drug and the nanocages. Based on the results of the simulation, the S_1, S_2, S_3, and S_4 states of CP/C_{24} complexes were adsorbed with −0.74 eV, −0.26 eV, −0.77 eV, and −0.41 eV adsorption energies at 2.353 Å, 2.632 Å, 2.367 Å, and 2.675 Å distances, respectively. Thus, S_3 is the most favourable state, *i.e.*, when the drug molecule is juxtaposed to the nanocage. The adsorption energy maintains an inversely proportional relationship with the interaction distance. After the adsorption of the CP drugs on the C_{24} nanocages, the nanocages remain almost symmetric (geometrically) as they were before adsorption, while the bond lengths varied slightly. If the value of the adsorption energy is greater than −0.8 eV then

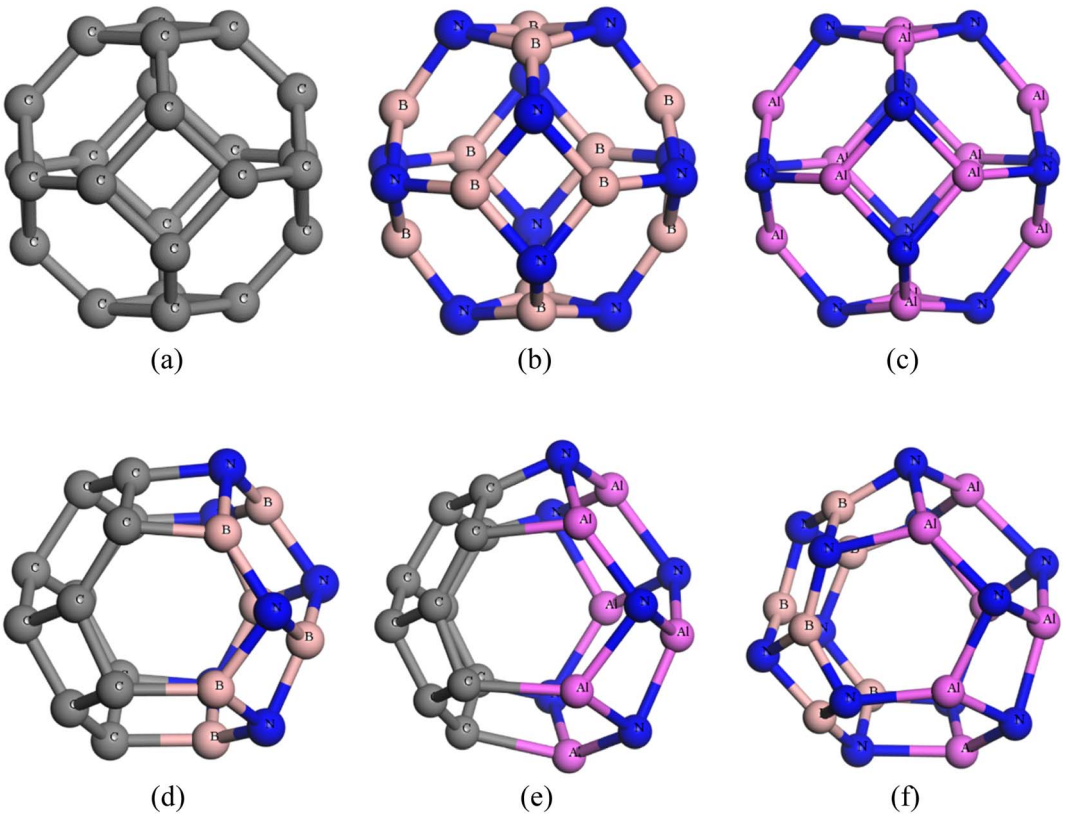

Fig. 1 Optimized structures of (a) C_{24}, (b) $B_{12}N_{12}$, (c) $Al_{12}N_{12}$, (d) C_{12}–B_6N_6, (e) C_{12}–Al_6N_6 and (f) B_6N_6–Al_6N_6.

it is called chemisorption, while less than −0.6 eV is referred to as physisorption.[53] According to this definition, no chemisorption was observed for CP/C_{24} complexes, all the adsorption energies of the four states exhibit physisorption. When cisplatin is inserted into the body environment, the main challenge, which the therapeutic of cisplatin meets is that the drug has to cross multiple biological barriers namely mouth mucosa, blood–brain barrier (BB), and gastrointestinal tract with the least generic accumulation. The efficacy of cisplatin therapeutics can be limited by premature release of the drug on undesired biological sites if there is weak binding between cisplatin and the studied nanocages. Therefore, strong binding between the drug and the nanocages is indispensable.

To verify the structural stability of the S_3 state of CP/C_{24}, vibrational frequency analysis was performed. The vibrational frequency analysis ensured that there was no existence of imaginary frequency for the S_3 state and the vibrational frequencies varied within the limit of 24.9 cm^{-1} to 3522 cm^{-1}. The energy gap (E_g), Frontier molecular orbital (FMO) analysis, and charge transfer (Q) (tabulated in Table 2) were studied to investigate the degree of sensitivity of C_{24} nanocages toward the CP drug. The FMO of the most favourable state of the CP/C_{24} complex (both top and side views) is depicted in Fig. SI2.† The HOMO and LUMO levels were randomly localized throughout the drug and the nanocage. For S_1, S_2, S_3, S_4 states of C_{24}, the LUMO energy (E_L) increases from −4.593 eV to −4.105 eV, −4.395 eV, −4.119 eV and −4.853 eV and HOMO energy (E_H) increased from −6.17 eV to −5.012 eV, −5.384 eV, −5.096 eV, −5.607 eV, respectively. Thus, energy gap of C_{24} decreases from 1.577 eV to 0.907 eV, 0.989 eV, 0.979 eV and 0.754 eV for S_1, S_2, S_3 and S_4 states, respectively. The calculated percentage reductions in the energy gap (% E_g) for S_1, S_2, S_3, and S_4 states were 42.5%, 37.286%, 37.9201%, and 52.1877%, respectively. A reduction in energy gap (E_g) leads to an exponential increment of conduction electron density, which is desired for targeted drug delivery. It should be taken into consideration that the conduction electron density (N_c) and energy gap (E_g) are related by the following relation:[54]

$$N = AT^{3/2}e^{\left(\frac{-E_g}{2KT}\right)} \quad (8)$$

where, K is the Boltzmann's constant = 1.380×10^{-23} m^2 kg s^{-2} k^{-1} and A (electrons per m^3 per $k^{3/2}$) is a constant.

Hirshfeld charge analysis to get an insight into the net charge transfer from the CP drug to the nanocages was performed. For S_1, S_2, S_3, and S_4 states, 0.260e, 0.097e, 0.266e, and 0.095e of charges, respectively, were transferred to the nanocages from the drug molecule. Hence, C_{24} nanocages acted as electron acceptors, whereas CP acted as the electron donor.

In the water medium, similar to the gas phase, attractive exothermic reactions between CP and C_{24} nanocage were observed. The maximum adsorption energy was found at about −0.769 eV when the drug molecule was placed parallel to the C_{24} nanocage at a distance of 2.287 Å from the nanocage. The

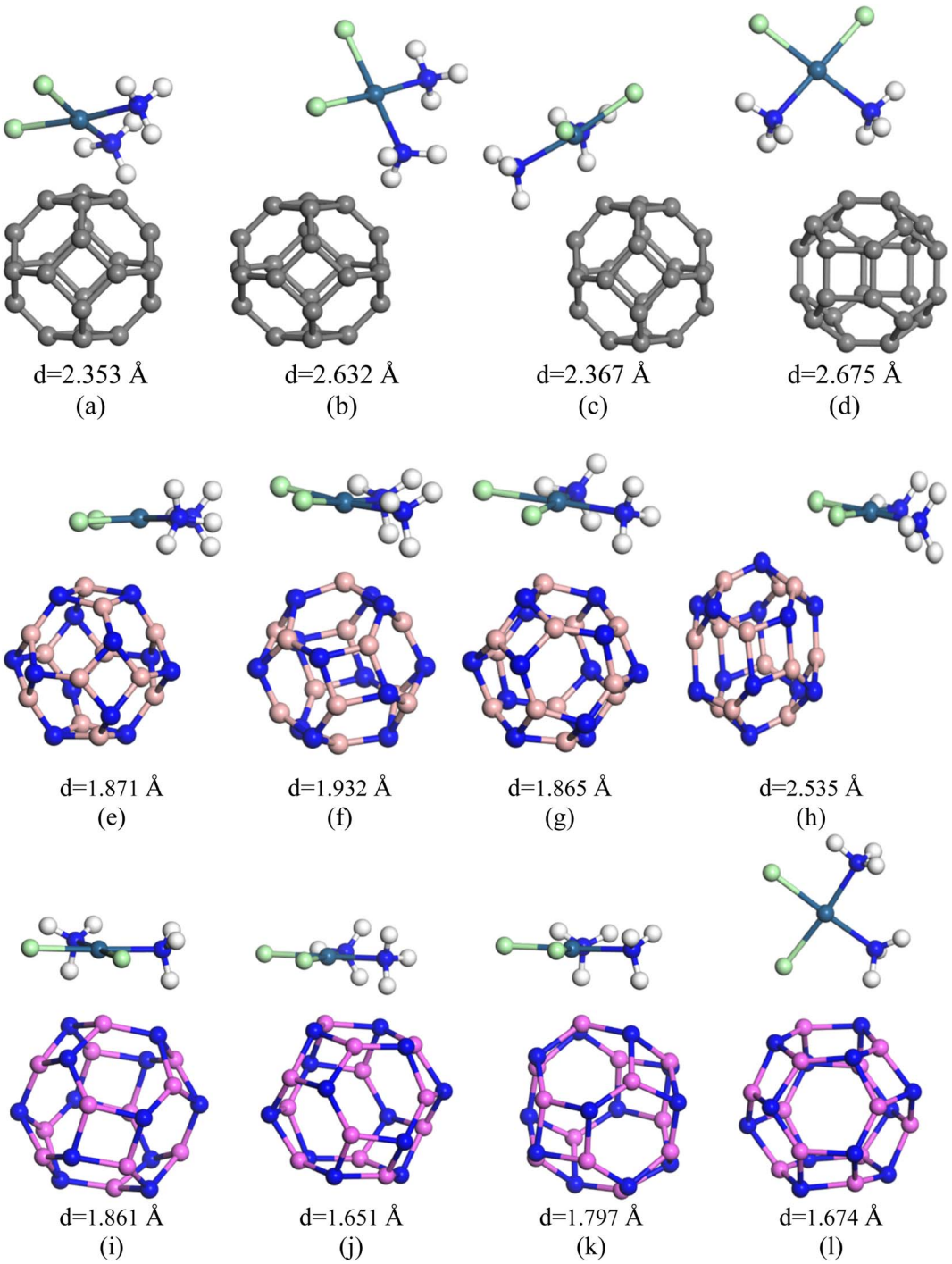

Fig. 2 Optimized structures of (a) S_1, (b) S_2, (c) S_3 and (d) S_4 states of CP/C_{24} complex; (e) S_1, (f) S_2, (g) S_3 and (h) S_4 states of CP/$B_{12}N_{12}$ complexes and (i) S_1, (j) S_2, (k) S_3 and (l) S_4 states of CP/$Al_{12}N_{12}$ complexes, respectively.

electrical properties (*e.g.*, E_g, HOMO, LUMO energies) change after having been CP adsorbed on C_{24} nanocage surfaces. The E_g of C_{24} was reduced by about 27.6% for the S_1 and 23.7% for the S_3 state after adsorption, while the energy gap reduction for the S_3 state was tremendous (~38%) in the gas phase as mentioned earlier. What is more, in the water phase, the drug is adsorbed on the nanocage at a closer distance than it was thought to be adsorbed previously in the gas phase. Therefore, in comparison with the gas phase, a slightly enhanced interaction between CP and C_{24} in the water phase was observed.

3.3. Adsorption of CP on $B_{12}N_{12}$ nanocage

From the above discussion, it is obvious that the degree of sensitivity exhibited by C_{24} towards the CP drug molecule is not intense enough. For this reason, we altered the C_{24} nanocage so

that we can obtain the $B_{12}N_{12}$ nanocage. After having the $B_{12}N_{12}$ nanocage optimized, CP drug molecules were adsorbed on it at different adsorption sites. Among the different orientations, four different states were considered, such as the ones we considered for the CP/C_{24} complex earlier. Adsorption energy and electronic properties were studied for the four states (Fig. 2). The CP drug was observed to be adsorbed on $B_{12}N_{12}$, 1.871 Å apart, and with an adsorption energy of −0.93 eV for the S_1 state.

The observed adsorption energies were −1.195 eV, −0.956 eV, and −0.485 eV for S_2, S_3 and S_4 states, respectively (tabulated in Table 2). Therefore, the S_2 state can be considered a more favourable state for the adsorption of CP on $B_{12}N_{12}$. According to the definition of adsorption energy, chemisorption occurs in the case of S_1, S_2, and S_3 states, while physisorption occurs in the case of the S_4 state. According to a previous theoretical investigation, it is a matter of fact that chemisorption is more favourable for the purpose of drug delivery.[55,56] $B_{12}N_{12}$ nanocages have been observed to deform near the adsorption site after the adsorption. A trend of increasing the 4CR–6CR junction bond lengths and of decreasing the 6CR–6CR junction bond lengths has been observed for all four states. According to the predictions of the Hirshfeld charge analysis, CP and $B_{12}N_{12}$ molecules act as electron donors and electron acceptors, respectively, by receiving an amount of charge (0.254*e*–0.364*e*) from CP. The ESP maps play a pivotal role as it gives a crystal clear insight into the visualization of the reactive sites depending on the distribution of charge density. In the ESP maps, the blue (positive domains) and the yellow (negative domains) colours signify relative inanition and accumulation of electronic charges, respectively. Fig. SI3(b)† depicts the ESP and EDM maps of the S_2 state of the CP/$B_{12}N_{12}$ complex. Between CP and $B_{12}N_{12}$, overlapping electron densities were observed which was confirmed by the electron density map (EDM). Additionally, the ESP map ensured that charge transfer occurred from CP to the $B_{12}N_{12}$ nanocage. E_H, E_L, E_g, and % ΔE_g are tabulated in Table 2. Significant changes in HOMO, LUMO energies and E_g of CP/$B_{12}N_{12}$ which are greater than CP/C_{24} complexes were observed. The HOMO and LUMO levels are localized on the CP drug molecule. After having CP adsorbed on the $B_{12}N_{12}$ surface, downward and upward shifts of E_H and E_L values for all states were observed. Increment in LUMO energy and a decrement in HOMO energy leads to the reduction of the energy gap. From 4.972 eV of the energy gap, drastic decrements to 2.564 eV, 2.806 eV, 2.582 eV, and 2.627 eV for S_1, S_2, S_3, and S_4 states, respectively, were observed. This trend of reduction in the band gap is supported by another finding by Saeid Onsori *et al.*, who investigated the adsorption of CP on $B_{12}N_{12}$ by employing B3LYP as a hybrid functional.[57] The changes in the energy gap (% ΔE_g) after adsorption of CP on $B_{12}N_{12}$ were 48.43% (S_1), 43.56% (S_2), 48.06% (S_3), and 47.16% (S_4), respectively. Reduced E_g increases the reactivity and sensitivity of $B_{12}N_{12}$ nanocages toward the CP drug. For CP/C_{24}, S_3 (which is the preferable state according to adsorption energy) the energy gap reduces to about 37.92% and in the CP/$B_{12}N_{12}$ complex, decrement in E_g occurs around 43.56%.

The adsorption energy for the S_2 state of CP/$B_{12}N_{12}$ in a water medium was observed at around −0.84 eV, which is coherent with the results of the gas medium. The CP molecule was observed to be adsorbed almost perpendicularly with $B_{12}N_{12}$ at a distance of 2.087 Å from the central top B atom. The CP drug molecule loses an amount of 0.175*e*. Analogous to the gas phase, the HOMO, LUMO, and E_g are not stagnated after adsorption. E_H is shifted from −7.144 eV to −6.283 eV, while the E_L is shifted from −2.077 eV to −3.13 eV for the S_2 state. The reduction of the energy gap observed was about 37.77% (S_2 state) after having the CP adsorbed. The above-mentioned fluctuations are indicative of a strong interaction between CP and $B_{12}N_{12}$ both in the gas and water phase.

3.4. Adsorption of CP on $A_{12}N_{12}$ nanocage

In view of enhancing the adsorption behaviour, C_{24} nanocages were further modified by substituting C atoms with equal proportions of Al and N atoms to form $Al_{12}N_{12}$ nanocage. After the optimization of $Al_{12}N_{12}$, CP drug was adsorbed on the surface of $Al_{12}N_{12}$ nanocages on different reactive sites and among them, 4 states were selected (Fig. 2) as we did before in the case of the previous two nanocages. For S_1, S_2, S_3 and S_4 states the obtained adsorption energies were −1.974 eV, −1.744 eV, 1.98 eV and −1.628 eV, respectively (Table 1). All four structures demonstrate chemisorption according to the definition of adsorption energy. The adsorption distances were observed at 1.861 Å (S_1), 1.651 Å (S_2), 1.797 Å (S_3), and 1.674 Å (S_4), respectively. The shortest adsorption distance corresponds to the S_2 state. The shortest adsorption distance between CP

Table 1 Calculated minimum interaction distances (*d*) in Å, adsorption energies (E_{ad}) in eV, and charge transfers (*Q*) in (*e*) between CP and our studied nano-cages

		Gas phase			Water phase		
Structure	State	*d*	E_{ad}	*Q*	*d*	E_{ad}	*Q*
CP/C_{24}	S_1	2.353	−0.744	0.260	2.306	−0.744	0.386
CP/C_{24}	S_2	2.632	−0.256	0.097	2.709	−0.256	0.058
CP/C_{24}	S_3	2.367	−0.769	0.266	2.287	−0.769	0.394
CP/C_{24}	S_4	2.675	−0.412	0.095	2.781	−0.412	0.052
CP/$B_{12}N_{12}$	S_1	1.871	−0.933	0.364	2.010	−0.712	0.463
CP/$B_{12}N_{12}$	S_2	1.932	−1.195	0.254	2.070	−0.838	0.355
CP/$B_{12}N_{12}$	S_3	1.865	−0.956	0.355	2.003	−0.738	0.445
CP/$B_{12}N_{12}$	S_4	2.535	−0.485	0.338	2.048	−0.522	0.636
CP/$Al_{12}N_{12}$	S_1	1.861	−1.974	0.130	1.938	−1.450	0.233
CP/$Al_{12}N_{12}$	S_2	1.651	−1.744	0.219	1.804	−1.447	0.305
CP/$Al_{12}N_{12}$	S_3	1.797	−1.98	0.122	1.932	−1.468	0.239
CP/$Al_{12}N_{12}$	S_4	1.674	−1.628	0.202	1.827	−1.394	0.321
CP/C_{12}–B_6N_6	S_1	2.077	−0.776	0.254	2.248	−0.446	0.378
CP/C_{12}–B_6N_6	S_2	2.426	−0.627	0.312	2.359	−0.395	0.298
CP/C_{12}–B_6N_6	S_3	1.910	−0.930	0.220	2.00	−0.688	0.575
CP/C_{12}–Al_6N_6	S_1	1.919	−1.933	0.149	2.478	−1.541	0.352
CP/C_{12}–Al_6N_6	S_2	1.797	−2.204	0.193	1.697	−1.655	0.372
CP/C_{12}–Al_6N_6	S_3	1.798	−2.215	0.192	1.897	−0.373	0.152
CP/B_6N_6–Al_6N_6	S_1	1.852	−1.993	0.221	2.067	−1.568	0.363
CP/B_6N_6–Al_6N_6	S_2	1.740	−2.136	0.312	2.336	−1.861	0.839
CP/B_6N_6–Al_6N_6	S_3	1.871	−2.115	0.173	2.147	−1.666	0.400

and $Al_{12}N_{12}$ nanocage of the most favourable state (S_3) depending upon the adsorption energy is about 1.797 Å, which is shorter than the interaction distances of the most favourable states of C_{24} (2.367 Å) and $B_{12}N_{12}$ (1.932 Å). The vibrational frequency analysis, which ensures structural stability unveils that there is no existence of any imaginary frequency for the S_3 state of CP/$Al_{12}N_{12}$ and the vibrational modes were found within the range of 35.5 cm^{-1} to 3513.4 cm^{1}. The Hirshfeld charge analysis indicates that, during the interaction, the CP drug molecule donates 0.122*e* charge to the $Al_{12}N_{12}$ nanocage.

The FMO maps of the S_3 state of the CP/$Al_{12}N_{12}$ complex are depicted in Fig. SI2(c) and (f).† Unlike CP/$B_{12}N_{12}$, the HOMO levels are localized on the $Al_{12}N_{12}$ nanocage and LUMO levels are located on the CP drug molecule. A trend of increasing HOMO and LUMO energies was observed for all the selected four states of CP/$Al_{12}N_{12}$ after adsorption. For S_1, S_2, S_3 and S_4 states, E_g decreases from 2.644 eV to 2.484 eV, 2.197 eV, 2.517 eV and 2.125 eV, respectively. The DOS spectra of $Al_{12}N_{12}$ are illustrated in Fig. 3(c), which depicts that no additional major peaks are generated after adsorption in the near vicinity of the Fermi level. EDM and ESP maps guarantee the event of electron density overlapping and hybridization between the CP and $Al_{12}N_{12}$ nanocage. Analogous to the gas media, for the S_3 state of $Al_{12}N_{12}$ the adsorption energy was found at about −1.468 eV. The charge transfer for this state is about 0.239*e* from CP to $Al_{12}N_{12}$. Significant variations in the electronic properties were also observed after the adsorption of CP on the $Al_{12}N_{12}$ nanocage. Thus, the adsorption behaviours of $Al_{12}N_{12}$ are preferable in both gas and water medium.

3.5. Adsorption of CP on C_{12}–B_6N_6 heteronanocage

Our inquiry still continues as we have customized the C_{24} nanocage by introducing 6 B and 6 N atoms at the cost of eliminating 12 C atoms to form the heteronanocage: C_{12}–B_6N_6 (Fig. 1(d)). It contains 5 types of bonds, which are C–C, B–B, B–C, C–N (at the junction of 4 and 6 component rings), and C–C (at the junction of 6 and 6 component rings) and, the magnitudes happen to be 1.502 Å, 1.383 Å, 1.553 Å, 1.497 Å, and 1.370 Å respectively. X. F. Fan *et al.* in 2008 investigated the structural

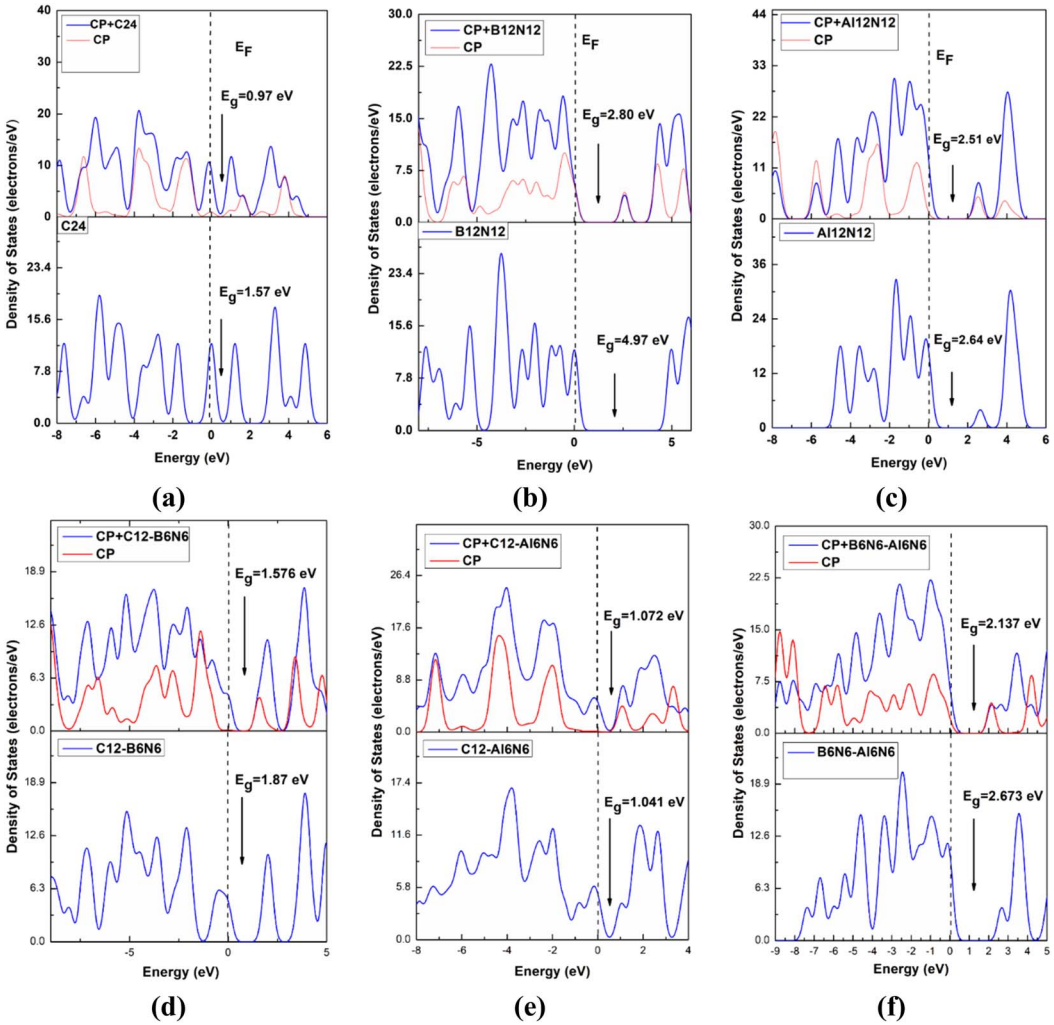

Fig. 3 The total and partial DOS for (a) C_{24}, (b) $B_{12}N_{12}$, (c) $Al_{12}N_{12}$, (d) C_{12}–B_6N_6, (e) C_{12}–Al_6N_6, and (f) B_6N_6–Al_6N_6 nano-cages before and after adsorption of CP drug molecule. The dotted line indicates the Fermi level.

stability of C_{12}–B_6N_6 fullerene by employing bond counting (BCR) rules coupled with a B3LYP-based DFT approach and confirmed the structural stability of the nanocage. This result further motivates our investigation of C_{12}–B_6N_6 and supports our vibrational mode analysis. In our vibrational frequency analysis, we have not found any imaginary frequencies. The range of the vibrational modes is 313.9–1577.6 cm^{-1}. Surprisingly, our calculated E_g of C_{12}–B_6N_6 agrees well with them.[58]

In the case of our hetero-nano-cage, we have considered three different states of the complexes, which are (i) adsorption on the C_{12} site, (ii) adsorption of the B_6N_6 site, and (iii) adsorption on their interface of the C_{12}–B_6N_6 hetero-nano-cage. Fig. 4 depicts the selected 3 states of the CP/C_{12}–B_6N_6 complex. The negative sign of the adsorption energies infers attractive interactions but the adsorption energies of both 2 states correspond to the physisorption range (except the S_3 in the gas phase) in both the gas and water phases, as tabulated in Table 1. In the gas phase, the adsorption energies are −0.776 eV, −0.627 eV, and −0.930 eV, and the interaction distances are 2.077 Å, 2.426 Å, and 1.910 Å, for the water phase, the E_{ad} are −0.446 eV, −0.395 eV, and −0.688 eV and the interaction distances are 2.248 Å, 2.359 Å and 2.00 Å for S_1, S_2, S_3 states, respectively. The Hirshfeld charge analysis predicts that 0.254*e*, 0.312*e*, and 0.220*e* charges are transported from the CP drug molecule to C_{12}–B_6N_6 nanocage for S_1, S_2, and S_3 states, respectively.

Upon FMO analysis, the data we have obtained are illustrated in Fig. SI4(a) and (d),† which indicate that the LUMO levels are located on the CP drug molecule and the HOMO levels are located on the C_{12}–B_6N_6 nanocage. The FMO analysis also suggests that the reduction in the energy gap is quite trivial, as tabulated in Table 2. The reductions in energy gaps are about 11.39% and 13.36% in the gas phase for S_1 and S_2 states, respectively. It is to be noted that the most stable complex (which is in terms of adsorption energy) S_3 has a reduction in the energy gap of about only 15.72% in the gas phase. The full and partial DOS spectra for the most stable complex are displayed in Fig. 3(d) and it implies that no dominant peaks are introduced in the near vicinity of the Fermi level. Therefore it is obvious for us to infer that, based on the electrical properties, the C_{12}–B_6N_6 nanocage shows the least preferable sensitivity towards the CP drug molecule.

3.6. Adsorption of CP on C_{12}–Al_6N_6 heteronanocage

To trace a better adsorbent for the targeted delivery of the CP drug molecule, we further adsorbed it on the surface of C_{12}–Al_6N_6 (Fig. 4). The optimized structure of C_{12}–Al_6N_6 contains 7 types of bonds and they are C–Al (1.966 Å), N–Al (1.867 Å), C–C shared between 4 and 6-CR (1.446 Å), C–C shared between 6 and 6-CR (1.81 Å), C–N shared between hetero-rings (1.361 Å), C–N shared between 4 and 6-CR (1.849 Å) and C–N shared between 6 and 6-CR (1.81 Å). The structural stability was confirmed by vibrational frequency analysis in which no imaginary frequency was found and the range of vibrational modes was 167.1–1571.8 cm^{-1} (Table 3). The calculated adsorption energies along with interaction distances and charge transfer for the 3 chosen states of CP/C_{12}–Al_6N_6 are tabulated in Table 1. Observations suggest that the CP drug molecule gets adsorbed on the surface of C_{12}–Al_6N_6 with adsorption energies of −1.933 eV, −2.204 eV, and −2.215 eV for S_1, S_2, and S_3 states in the gas phase with the interaction distances of 2.492 Å, 1.79 Å, and 1.798 Å, respectively. Our calculated E_g of C_{12}–Al_6N_6 agrees well with the findings of Paul *et al.*[59] It may apparently seem that the S_3 state is the most stable complex, but in the water phase, this state has an adsorption energy of −0.373 eV with an interaction distance of 1.897 Å. While in the water phase, the S_2 state shows adsorption energy (−1.655 eV), which is way too consistent compared with the S_3 state. The interaction distance of the S_2 state is the shortest in both water and gas media, as we can see from Table 1. The Hirshfeld charge analysis predicts that an appreciable amount of charge is transferred from the CP drug molecule to the nanocage, which is 0.372*e* (in water medium) and 0.193*e* (in gas medium) for the S_2 state. The other two states have lower charge transfers, as suggested by the Hirshfeld charge analysis. The HOMO levels are situated at the nanocage and the LUMO levels are situated at the drug molecule, as can be seen from the FMO analysis in Fig. SI4(b) and (e).† Table 2 shows the variation of the electronic parameters of the nanocages after adsorption. In the gas phase, only the S_1 state exhibits a reduction in the energy gap of 13.5%, while the S_2 and S_3 states exhibit an increment of the energy gap of 2.9% and 2.4%, respectively. However, this scenario is exactly the opposite in the water phase, where the S_1 state undergoes an increment in the energy gap of 3.7%, while the S_2 and S_3 states exhibit a decrement in the energy gap of 2% and 3.5%, respectively. Full and partial DOS spectra analysis as depicted in Fig. 3(e) shows that no extra dominant peaks are generated near the Fermi level. It can be concluded that C_{12}–Al_6N_6 nanocages show less sensitivity toward the CP drug molecule.

3.7. Adsorption of CP on B_6N_6–Al_6N_6 heteronanocage

Ultimately, in search of a potent adsorbent for the CP drug to be adsorbed, we further modified the previous nanocage by removing all the carbon atoms and introducing 6 N and 6 B atoms in the place of the C atoms of the nanocage to form B_6N_6–Al_6N_6. We studied the bond types of the nanocage and found 6 types of bonds, which are B–N (1.427 Å) shared between 6 and 6-CR, B–N (1.506 Å) shared between 4-CR and 6-CR (hetero ring), B–N (1.481 Å) shared between 4 and 6-CR, Al–N (1.863 Å) shared between 4 and 6-CR, Al–N (1.841 Å) shared between 4 and 6-CR (hetero), Al–N (1.8 Å) shared between 6 and 6-CR. The positive vibrational modes were found in the range of 179.1–1385.6 cm^{-1} which verified the structural stability of the heteronanocage. Exceptionally high negative adsorption energies were observed, which are listed in Table 1 along with interaction distances. The main contrast between the previously studied nanocages and B_6N_6–Al_6N_6 nanocage is that B_6N_6–Al_6N_6 exhibits preferable high negative E_{ad} in both gas and water media for all the states as well as the interaction distance is optimum. In the gas phase, S_1 and S_3 states both exhibit E_{ad} of −1.852 eV and 1.871 eV, respectively, which is slightly higher than the E_{ad} of the S_2 state (−1.740 eV). On the other hand, the

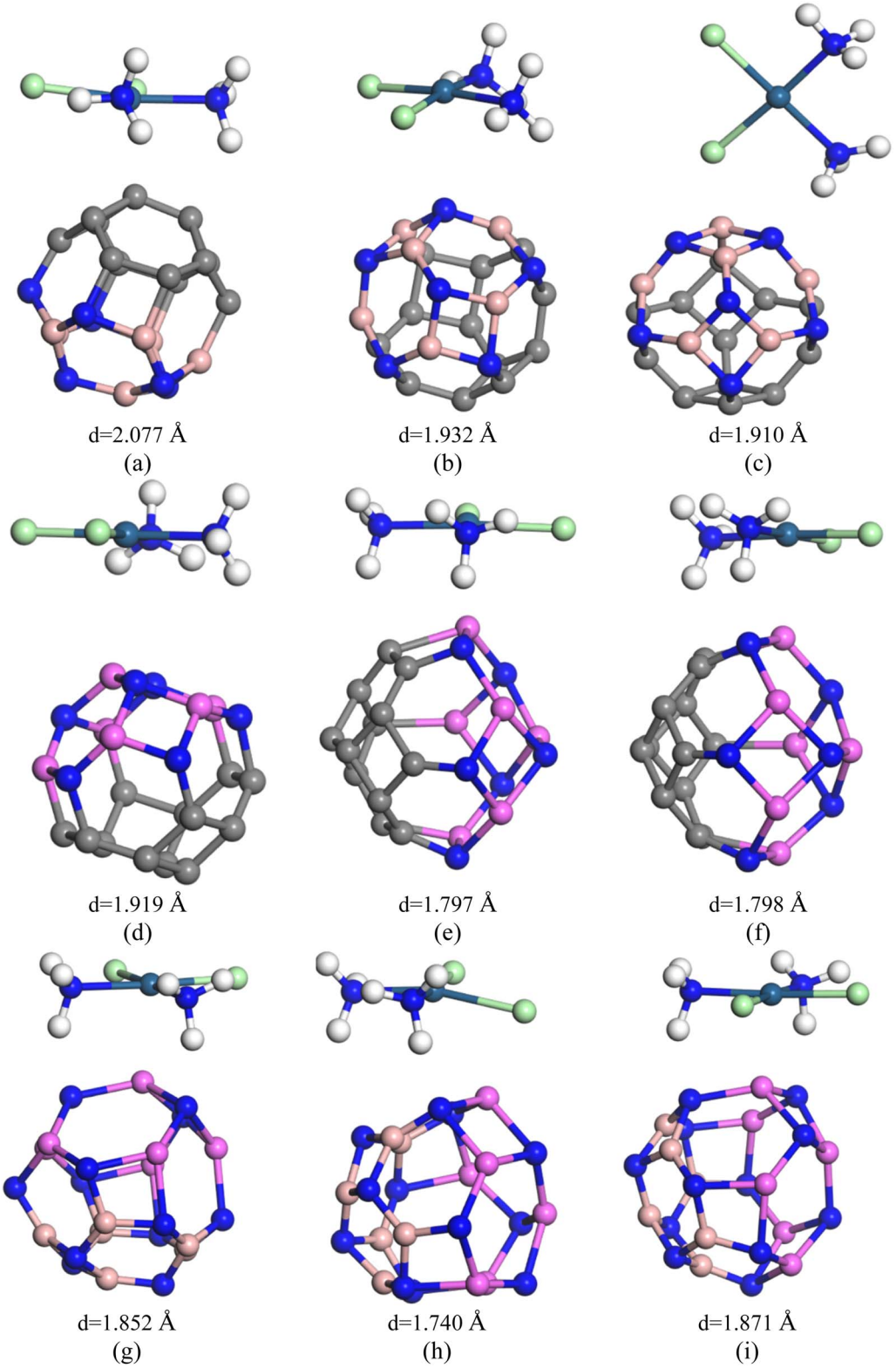

Fig. 4 Optimized structures of (a) S_1, (b) S_2, and (c) S_3 states of CP/C_{12}–B_6N_6 complexes; (d) S_1, (e) S_2, and (f) S_3 states of CP/C_{12}–Al_6N_6 complexes and (g) S_1, (h) S_2 and (i) S_3 states of CP/B_6N_6–Al_6N_6 complexes, respectively.

S_2 state exhibit an adsorption energy of −1.861 eV, which is far better than the adsorption energies of both the S_1 and S_3 states (−1.568 eV and −1.666 eV, respectively). The Hirshfeld charge analysis unveils that a large proportion of charge transfer occurs for the most stable state (*i.e.*, S_2), especially in the water phase, the amount of charge transferred from CP to the nanocage is

Table 2 Calculated HOMO energies (E_{HOMO}), LUMO energies (E_{LUMO}), HOMO–LUMO energy gap (E_g) in eV, change in energy gap (% ΔE_g), and dipole moment (D.M) in Debye (*D*) of the studied complexes in both gas and water phases

		Gas phase					Water phase				
Structure	State	E_{HOMO}	E_{LUMO}	E_g	% E_g	D.M	E_{HOMO}	E_{LUMO}	E_g	% E_g	D.M
C_{24}		−6.17	−4.593	1.577		0	−5.714	−4.492	1.22		0
CP/C_{24}	S_1	−5.012	−4.105	0.907	−42.4	9.33	−5.038	−4.153	0.885	−27.5	17.39
CP/C_{24}	S_2	−5.384	−4.395	0.989	−37.2	9.22	−5.557	−4.457	1.1	−9.9	15.19
CP/C_{24}	S_3	−5.098	−4.119	0.979	−37.9	9.07	−5.073	−4.141	0.932	−23.7	17.12
CP/C_{24}	S_4	−5.607	−4.853	0.754	−52.1	6.89	−5.683	−4.59	1.093	−10.5	17.12
$B_{12}N_{12}$		−7.132	−2.16	4.972		0	−5.506	−2.461	3.05		0
CP/$B_{12}N_{12}$	S_1	−5.791	−3.227	2.564	−48.4	11.52	−5.763	−2.88	2.883	−43.4	18.45
CP/$B_{12}N_{12}$	S_2	−6.11	−3.304	2.806	−43.5	8.99	−6.283	−3.13	3.153	−37.7	16.23
CP/$B_{12}N_{12}$	S_3	−5.789	−3.207	2.582	−48.0	11.64	−5.784	−2.876	2.908	−42.6	18.25
CP/$B_{12}N_{12}$	S_4	−5.746	−3.119	2.627	−47.1	14.19	−5.74	−2.993	2.747	−45.7	24.29
$Al_{12}N_{12}$		−5.696	−3.052	2.644		0	−5.506	−2.461	3.045		0
CP/$Al_{12}N_{12}$	S_1	−5.482	−2.998	2.484	−6.0	7.41	−5.69	−3.019	2.671	−1.5	14.05
CP/$Al_{12}N_{12}$	S_2	−5.176	−2.979	2.197	−16.9	9.75	−5.55	−2.954	2.596	−4.2	16.63
CP/$Al_{12}N_{12}$	S_3	−5.502	−2.985	2.517	−4.8	7.36	−5.701	−3.026	2.675	−1.3	14.14
CP/$Al_{12}N_{12}$	S_4	−5.155	−3.03	2.125	−19.6	10.17	−5.494	−2.942	2.552	−5.8	16.54
C_{12}–B_6N_6		−5.735	−3.856	1.87		1.95	−5.732	−3.809	3.00		3.44
CP/C_{12}–B_6N_6	S_1	−5.184	−3.527	1.65	−11.3	7.3	−6.052	−3.228	2.82	−6.1	21.9
CP/C_{12}–B_6N_6	S_2	−5.275	−3.655	1.62	−13.3	10.1	−5.036	−3.402	1.63	−45.6	26.6
CP/C_{12}–B_6N_6	S_3	−4.983	−3.407	1.57	−15.7	11.9	−6.045	−3.288	2.75	−8.3	17.4
C_{12}–Al_6N_6		−4.525	−3.484	1.041		8.5	−4.893	−3.496	1.39		13.3
CP/C_{12}–Al_6N_6	S_1	−4.39	−3.49	0.9	−13.5	12.2	−4.729	−3.28	1.44	3.7	24.2
CP/C_{12}–Al_6N_6	S_2	−4.365	−3.293	1.07	2.9	6.0	−4.686	−3.267	1.41	−2.0	13.9
CP/C_{12}–Al_6N_6	S_3	−4.369	−3.303	1.06	2.4	5.4	−4.892	−3.544	1.34	−3.5	23.4
B_6N_6–Al_6N_6		−5.912	−3.239	2.67		7.3	−6.306	−3.298	3.0		11.1
CP/B_6N_6–Al_6N_6	S_1	−5.757	−3.484	2.27	−14.9	11.3	−6.052	−3.228	2.82	−6.1	21.9
CP/B_6N_6–Al_6N_6	S_2	−5.337	−3.2	2.13	−20.0	4.9	−5.036	−3.402	1.63	−45.6	26.6
CP/B_6N_6–Al_6N_6	S_3	−5.737	−3.463	2.27	−14.9	8.98	−6.045	−3.288	2.75	−8.3	17.4

about 0.839*e*, which is the largest amount of charge transfer we have observed so far in this investigation. Results obtained from the FMO analysis are listed in Table 2. For the S_1 and S_3 states, the reduction in the energy gap is about 14.9%, while the S_2 state shows a reduction of about 20%. In the water phase, we can see the S_2 state undergoes an outstanding reduction of 45.6% in E_g. The LUMO and HOMO profiles of the S_2 state show that the HOMO levels are located in both the drug and nanocage while the LUMO levels are located on the drug molecule only. The ESP and EDM maps of the most stable complex of CP/B_6N_6–Al_6N_6 are illustrated in Fig. SI5(c) and (f).† The full and partial DOS spectra are illustrated in Fig. 3(f) which, ensures the energy gap reduction phenomenon of the S_2 state.

Table 3 Ranges of vibrational modes in cm^{-1} of our most stable states of the complexes

Structure	Vibrational mode ranges (cm^{-1})
CP/C_{24}/S_3	24.9–3522.1
CP/$B_{12}N_{12}$/S_2	64.4–3400.7
CP/$Al_{12}N_{12}$/S_3	35.5–3513.4
CP/C_{12}–B_6N_6/S_3	14.7–3526
CP/C_{12}–Al_6N_6/S_2	23.6–3523.4
CP/B_6N_6–Al_6N_6/S_2	40.6–3525.7

3.8. Quantum molecular descriptors and dipole moment

In Table 4, global descriptors of the complexes are tabulated to gain a better insight into the stability as well as the reactivity of our complexes under study. The resistance to the deformation of alignment of the electron cloud of atoms, ions, or molecules is defined as global hardness (η). The stability of the structure increases with increasing global hardness thereby leading to a substantial decrement in reactivity.[53] Another vital parameter is the electrophilicity index (ω) which defines the electrophilic behaviour of a compound. The electrophilicity index (ω) maintains an inversely proportional relationship with global hardness (η). The higher the electrophilicity index and softness, the higher the reactivity of the complexes. In our investigation, a decreasing trend of hardness and increasing trend of electrophilicity index (ω) and global softness (S) are observed.

The calculated hardnesses for C_{24}, $B_{12}N_{12}$, and $Al_{12}N_{12}$ are 0.755 eV, 2.486 eV, and 1.322 eV, respectively. However, the hardness decreases from 0.755 eV to 0.377–0.494 eV for C_{24}, from 2.486 eV to 1.282–1.403 eV for $B_{12}N_{12}$, from 1.322 eV to 1.062–1.258 eV after adsorption. To sum up, the chemical stability of the complexes of CP/C_{24}, CP/$B_{12}N_{12}$, and CP/$Al_{12}N_{12}$ decreases but reactivity increases. Furthermore, the computed values of softness and electrophilicity index of the three nanocages were observed to shift to higher values, which is an indication of the increased reactivity. The global softness is

Table 4 Computed chemical potential (μ), global hardness (η), electrophilicity index (ω), and global softness (S) of the studied complexes

Structure	State	μ (eV)	η (eV)	ω (eV)	S (eV^{-1})
CP		−3.694	1.334	5.114	0.374
C_{24}		−5.381	0.788	18.364	0.634
CP/C_{24}	S_1	−4.558	0.453	22.910	1.102
CP/C_{24}	S_2	−4.889	0.494	24.173	1.011
CP/C_{24}	S_3	−4.608	0.486	21.693	1.021
CP/C_{24}	S_4	−5.23	0.377	36.277	1.326
$B_{12}N_{12}$		−4.646	2.486	4.341	0.201
CP/$B_{12}N_{12}$	S_1	−4.509	1.282	7.929	0.390
CP/$B_{12}N_{12}$	S_2	−4.707	1.403	7.895	0.390
CP/$B_{12}N_{12}$	S_3	−4.498	1.291	7.835	0.387
CP/$B_{12}N_{12}$	S_4	−4.432	1.313	7.478	0.380
$Al_{12}N_{12}$		−4.374	1.322	7.235	0.378
CP/$Al_{12}N_{12}$	S_1	−4.24	1.242	7.237	0.402
CP/$Al_{12}N_{12}$	S_2	−4.077	1.098	7.567	0.455
CP/$Al_{12}N_{12}$	S_3	−4.243	1.258	7.154	0.397
CP/$Al_{12}N_{12}$	S_4	−4.092	1.062	7.881	0.470
C_{12}–B_6N_6		−4.8	0.935	12.320	0.534
CP/C_{12}–B_6N_6	S_1	−4.355	0.828	11.448	0.603
CP/C_{12}–B_6N_6	S_2	−4.465	0.81	12.306	0.617
CP/C_{12}–B_6N_6	S_3	−4.195	0.788	11.166	0.634
C_{12}–Al_6N_6		−4.004	0.520	15.404	0.960
CP/C_{12}–Al_6N_6	S_1	−3.94	0.45	17.248	1.111
CP/C_{12}–Al_6N_6	S_2	−3.829	0.536	13.676	0.932
CP/C_{12}–Al_6N_6	S_3	−3.836	0.533	13.803	0.938
B_6N_6–Al_6N_6		−4.575	1.336	7.832	0.374
CP/B_6N_6–Al_6N_6	S_1	−4.620	1.136	9.392	0.439
CP/B_6N_6–Al_6N_6	S_2	−4.268	1.068	8.526	0.467
CP/B_6N_6–Al_6N_6	S_3	−4.6	1.137	9.305	0.439

incremented from 0.634 eV^{-1} to 1.021 eV^{-1}, from 0.201 eV^{-1} to 0.356 eV^{-1}, from 0.378 to 0.397 eV^{-1} for the S_3, S_2, and S_3 states of CP/C_{24}, CP/$B_{12}N_{12}$ and CP/$Al_{12}N_{12}$, respectively. The computed hardness of C_{12}–B_6N_6, C_{12}–Al_6N_6, and B_6N_6–Al_6N_6 nanocages are 0.935 eV, 0.520 eV, and 1.336 eV, respectively. C_{12}–B_6N_6 and B_6N_6–Al_6N_6 nanocages were observed to have a reduced global hardness (0.788 eV and 1.068 eV, respectively), while the hardness of the C_{12}–Al_6N_6 nanocage increases to 0.536 eV after adsorption. With an initial value of global softness of 0.534 eV^{-1} and 0.374 eV^{-1}, C_{12}–B_6N_6 and B_6N_6–Al_6N_6 nanocages exhibited an increment of 0.634 eV^{-1} and 0.467 eV^{-1}, respectively, while C_{12}–Al_6N_6 showed a decrement in its softness (from 0.960 eV^{-1} to 0.932 eV^{-1}). A trend of the decreasing electrophilicity index was observed in the case of C_{12}–B_6N_6 and C_{12}–Al_6N_6 (except for the S_1 state) nanocages, while an increasing trend of electrophilicity index was observed in the case of B_6N_6–Al_6N_6 (except for the S_2 state) nanocage.

The measurement of symmetricity of the complex dipole moment (D.M) is a significant study. The dipole moment study in the water phase provides a deeper insight into the solubility of a complex. The higher value of dipole moment indicates higher solubility, reactivity, and higher transit of charge between the drug and nanocage.[60–62] Through the dipole moment study, we investigated the asymmetry of the charge distribution of our complexes. The calculated D.M for C_{24}, $B_{12}N_{12}$, and $Al_{12}N_{12}$ were all 0 D. On the other hand, D.M increases outstandingly for all the preferable states after adsorption (Table 2). After adsorption, the solubility of the complexes in the human body is thus ensured by a noticeable rise in the dipole moment values. In the water medium, the computed dipole moments of the nanocages were also 0 D. After adsorption in the water medium, the dipole moments were highly increased by about 17.13 D, 16.23 D and 14.14 D for S_3, S_2, and S_3 states of CP/C_{24}, CP/$B_{12}N_{12}$ and CP/$Al_{12}N_{12}$ complexes, respectively. Unlike C_{24}, $B_{12}N_{12}$, or $Al_{12}N_{12}$ nanocages, the dipole moments of C_{12}–B_6N_6, C_{12}–Al_6N_6, and B_6N_6–Al_6N_6 nanocages are non-zero before adsorption and the values happen to be 1.95 D, 8.54 D, and 7.39 D, respectively. The dipole moment of C_{12}–B_6N_6 increases to 11.992 D, while the dipole moments of C_{12}–Al_6N_6 and B_6N_6–Al_6N_6 tend to decrease to 6.036 D and 4.943 D after adsorption from their initial values before adsorption. However, this scenario in the water phase is obviously different since all three stable complexes of C_{12}–B_6N_6, C_{12}–Al_6N_6, and B_6N_6–Al_6N_6 show dipole moment values of 23.39 D, 13.96 D, and 26.66 D (after adsorption) incremented from their initial dipole moment values of 3.44 D, 13.39 D, and 11.14 D (before adsorption).

3.9. Work function analysis

To justify the sensitivity of the CP drug molecule toward the nanocages, the work function (φ) study is a pivotal investigation. Whether the CP drug is affecting or not the work function of the nanocages was studied in this analysis. The work function is referred to be the minimum thermodynamic work (energy) required to remove an electron from a solid surface to vacuum instantaneously and is defined by the following relation,[63]

$$\varphi = V_{e(+\infty)} - E_F \quad (9)$$

Here, E_F and φ correspond to the Fermi level and work function, $V_{e(+\infty)}$ is the electrostatic potential of an electron far away from the surface, which we can consider being zero *i.e.*, $V_{e(+\infty)} = 0$. Hence, the work function is numerically equal to the Fermi-level energy, $\varphi = -E_f$.

The field emission characteristics of the nanocages are altered by varying the work function, which may consequently end up changing the gate voltage.[64,65] This is well explained by Richardson Dushman equation[66]

$$j = AT^2 e^{(-\varphi/KT)} \quad (10)$$

j = electron current density emitted from the surface of a material. K = Boltzmann constant. T = Temperature. A = Richardson constant (A m^{-2}).

The change in the work function after adsorption can be calculated using the following formula:

$$\Delta\varphi = \frac{\varphi_f - \varphi_i}{\varphi_i} \times 100\% \quad (11)$$

where, φ_i = initial work function of nanocages (before adsorption), φ_f = final work function of nanocages (after adsorption of the drug molecule).

Tables SI1 and SI2† illustrate the computed work function values. In our study, the work function of C_{24} was found about 5.12 eV. Observations indicate that during the adsorption of the drug on our nanocages under study, work functions are outstandingly fluctuating. Negative and positive signs of the variation of work function (φ) indicate increment and decrement of φ of adsorbents after adsorbing CP, respectively. In the gas phase, C_{24} and $Al_{12}N_{12}$ φ were observed to increase about 9.824% and 1.365% and decrease about 0.71% for $B_{12}N_{12}$ after the adsorption of CP. φ is increased by about 8.672% and 2.673% for C_{24} and $Al_{12}N_{12}$ and decreased by about 0.967% for $B_{12}N_{12}$ after the adsorption of CP drug in the water medium. Therefore, according to work-function analysis, C_{24} and $Al_{12}N_{12}$ nanocages show higher sensitivity than $B_{12}N_{12}$ towards the CP drug. For all three stable complexes, the nanocages tend to exhibit a decrement in their work function after adsorption. In the gas phase, the decrements was observed to be about 5.97%, 2.63%, and 7.04% for the S_3, S_2, and S_3 states of CP/C_{12}–B_6N_6, CP/C_{12}–Al_6N_6 and CP/B_6N_6–Al_6N_6 complexes, respectively. Similarly, in the water phase, we observed analogous decrement of about 5.19%, 0.86%, and 8.27% for S_3, S_2, and S_3 states of CP/C_{12}–B_6N_6, CP/C_{12}–Al_6N_6 and CP/B_6N_6–Al_6N_6 complexes, respectively. Upon the work function analysis, it was quite obvious to infer that C_{12}–B_6N_6 and B_6N_6–Al_6N_6 showed less sensitivity toward the CP drug molecule. To draw a conclusion, in view of the work function analysis among the studied nanocages, C_{24} shows better sensitivity toward CP.

3.10. COSMO surface analysis

Previously, we have discussed how the presence of solvent dominates the adsorption process of CP on nanocages under study through energy calculations, the variation of electronic properties, dipole moment analysis, *etc.* in the water medium to mimic the body's biochemical environment and to reach experimental conditions. To obtain a more detailed insight into the polarity of the drug and nanocage complexes, a COSMO surface analysis was performed. Fig. 5 shows the COSMO surfaces of C_{24}, $B_{12}N_{12}$, $Al_{12}N_{12}$, C_{12}–B_6N_6, C_{12}–Al_6N_6, and B_6N_6–Al_6N_6. Whereas, Fig. 6 depicts the illustrations of COSMO surface analysis of drug–nanocage complexes under study. The green segments correspond to non-polar neutral parts of the molecules. The blue areas denote the highly positive region. Therefore, they form the hydrogen bond donor (HBD) region to the solvent media. Conversely, the red regions report the highly negative region, which is the hydrogen bond acceptor (HBA) region to the solvent. As we can see from Fig. 5, the COSMO surface of C_{24} is almost green everywhere, which indicates that the polarity of C_{24} is neutral before adsorption. The HBD regions are situated over the nitrogen atoms in the case of both $B_{12}N_{12}$ and $Al_{12}N_{12}$ nanocages. While the HBA regions are located on the B and Al atoms. In the case of the C_{12}–B_6N_6 and C_{12}–Al_6N_6 heteronanocages, the HBD regions are located on the C_{12} portion of the nanocages, while HBA regions are located on the B_6N_6 and Al_6N_6 portions of the nanocages, respectively. Similarly, we can observe the locations of the HBA and HBD regions in the case of the B_6N_6–Al_6N_6 nanocage. After

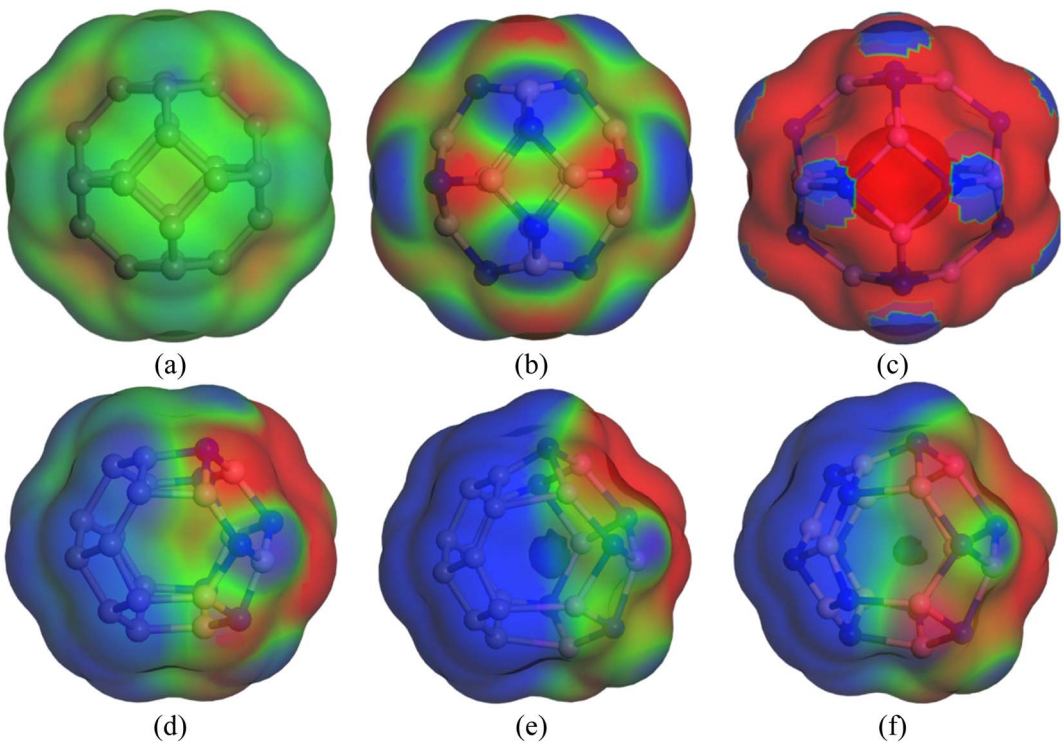

Fig. 5 COSMO surfaces for (a) C_{24}, (b) $B_{12}N_{12}$, (c) $Al_{12}N_{12}$, (d) C_{12}–B_6N_6, (e) C_{12}–Al_6N_6 and (f) B_6N_6–Al_6N_6, respectively.

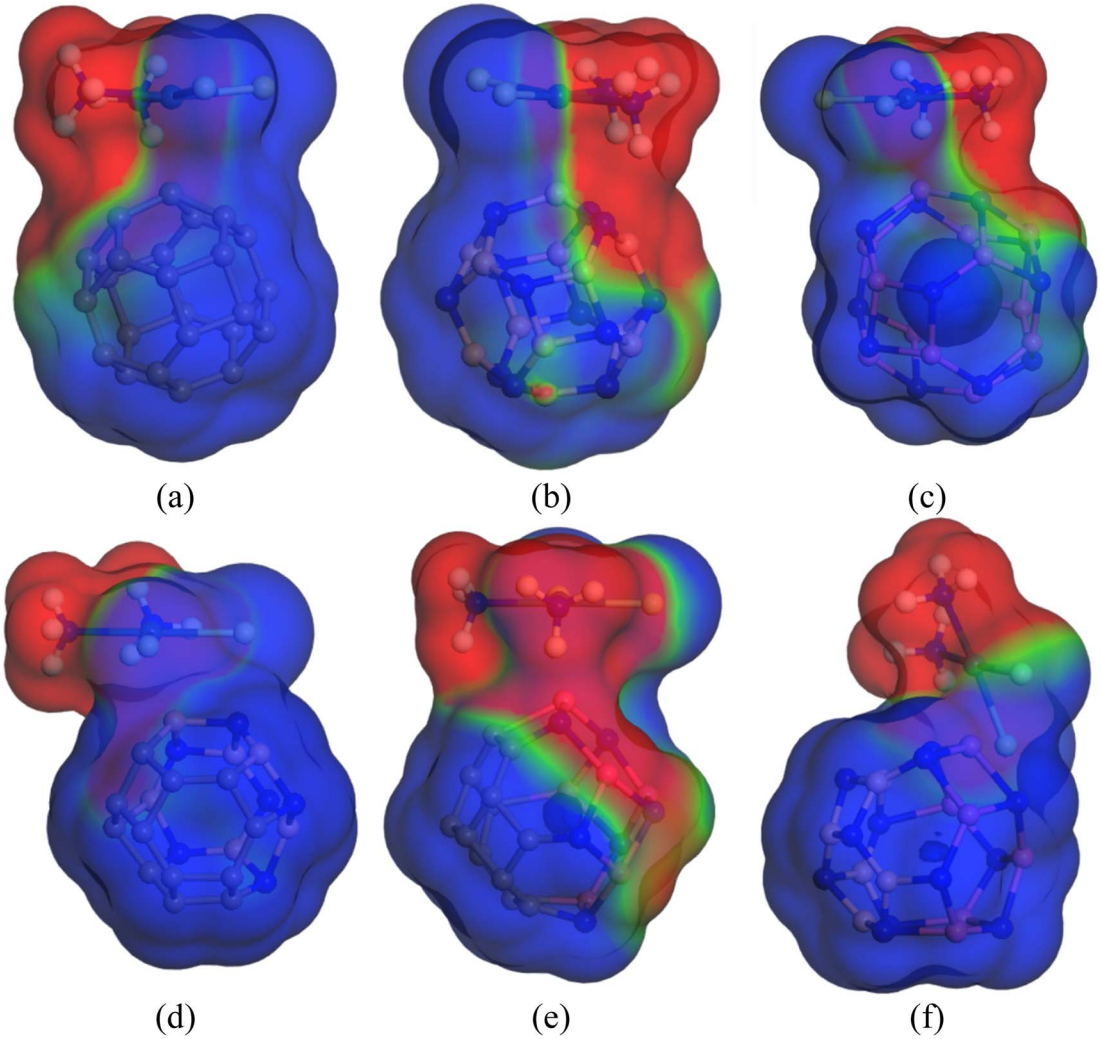

Fig. 6 COSMO surfaces of our most stable states (a) CP/C_{24} (S_3), (b) CP/$B_{12}N_{12}$ (S_2), (c) CP/$Al_{12}N_{12}$ (S_3), (d) CP/C_{12}–B_6N_6 (S_3), (e) CP/C_{12}–Al_6N_6 (S_2) and (f) CP/B_6N_6–Al_6N_6 (S_2), respectively.

adsorption, it is clear from Fig. 6 that NH_3 portions of the CP drug molecule denote the negative polarity region in the case of all the complexes, while the majority portion of the nanocages denotes the positive polarity region. Finally, it can be inferred that CP adsorption on the nanocages drastically enhanced the polarity of the nanocages, which is coherent with our dipole moment analysis.

3.11. QTAIM analysis

QTAIM analysis was performed since we were interested in explaining the intermolecular interactions and the bonding types. The quantum theory of atoms is an indispensable tool as it helps to visualize the non-covalent, hydrogen, or halogen-type chemical interactions.[67] The molecular graphs for the most stable complexes in the water phase are depicted in Fig. 7. The figure demonstrates all the critical points and bond paths between the drug and the nanocages. As can be seen from Table 5, the charge density (ρ_b) values range from 0.0212–0.0818 a.u. and the Laplacian of charge density ($\nabla^2\rho_b$) values lie within −1.3588 and 0.1301 a.u. A positive value of $\nabla^2\rho_b$ is indicative of non-covalent interaction, *i.e.*, a closed shell interaction (including van der Waals and ionic interaction), whereas a negative value of $\nabla^2\rho_b$ implies a shared interaction in the same way as in covalent interaction. It is obvious from Table 5 that all Laplacian of charge density values are positive except for BCP 50 of CP/C_{12}–B_6N_6 and BCP 82 of CP/B_6N_6–Al_6N_6. The ratio of $-G_b/V_b$ also plays an unquestionable role in determining the bonding nature. For $-G_b/V_b$ positive and greater than 1, the interaction is assumed to be purely non-covalent, while the bond is considered covalent if the ratio is smaller than 0.5. The total electron energy density H_b at a BCP can play a decisive role in getting a better insight into the bond type and interaction. A positive value of total electron energy density (H_b) indicates

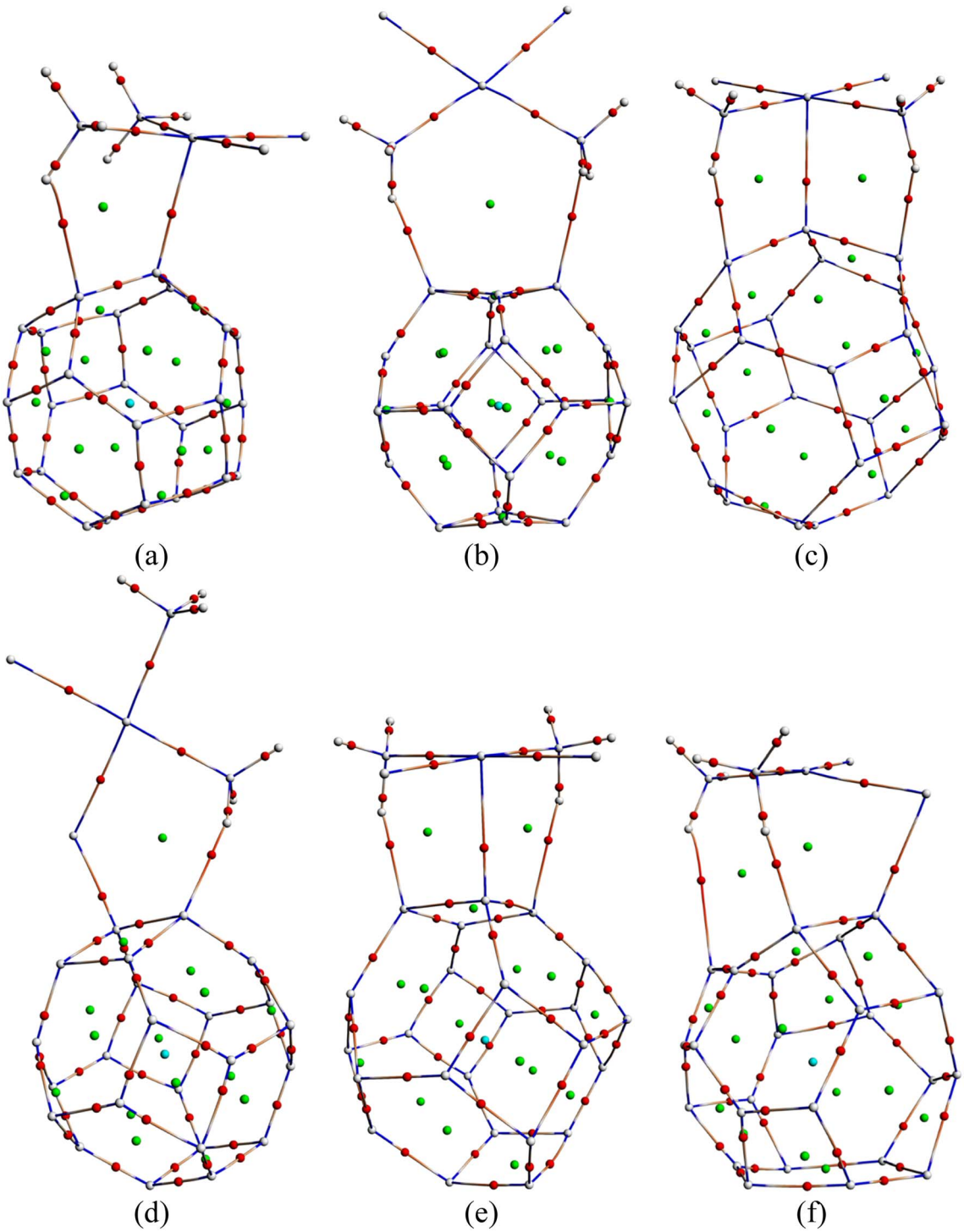

Fig. 7 The molecular graphs of the studied (a) CP/C_{24} (S_3), (b) CP/$B_{12}N_{12}$ (S_2), (c) CP/$Al_{12}N_{12}$ (S_3), (d) CP/C_{12}–B_6N_6 (S_3), (e) CP/C_{12}–Al_6N_6 (S_2) and (f) CP/B_6N_6–Al_6N_6 (S_2) complexes, respectively. The bond critical points are indicated by red solid circles.

a closed-shell interaction, whereas, a negative H_b indicates a covalent bond.[68] For BCP-46 CP/C_{24} and BCP-68 CP/$B_{12}N_{12}$, $H_b > 0$, $\nabla^2\rho_b > 0$, and $-G_b/V_b > 1$ indicating these interactions to be non-covalent in nature. For BCP-42 CP/C_{24}, BCP-44 CP/$B_{12}N_{12}$, BCP-59, 75, 85 CP/$Al_{12}N_{12}$, BCP-46 CP/C_{12}–B_6N_6, BCP-54, 72 CP/C_{12}–Al_6N_6, BCP-65, 77, 82 CP/B_6N_6–Al_6N_6, $H_b<0$, $-G_b/V_b < 1$ and $\nabla^2\rho_b > 0$, which is an indicator of stronger interaction with partially covalent character. It is worth pointing out that the obtained QTAIM results for the CP/$B_{12}N_{12}$ and CP/B_6N_6–Al_6N_6 complexes are in good agreement with the interactions predicted by the adsorption energy calculation, FMO analysis, DOS spectra analysis.

Table 5 Topological parameters, $-G_b/V_b$ ratio, total electron energy density (H_b), potential electron energy density (V_b), kinetic electron energy density (G_b), Laplacian of electron density ($\nabla^2\rho_b$), and electron density (ρ_b) at the bond critical points of the investigated complexes in a.u

Complex	BCP	ρ_b	$\rho_b \times 10^3$	$\nabla^2\rho_b$	G_b	V_b	H_b	$-G_b/V_b$
CP/C_{24} (S_3)	42	0.0653	65.337	0.1054	0.0480	−0.0696	−0.0216	0.68917
	46	0.0212	21.248	0.0572	0.0142	−0.0141	0.0009	1.0064
CP/$B_{12}N_{12}$ (S_2)	44	0.0372	37.279	0.1144	0.0310	−0.0334	−0.0024	0.9280
	68	0.0222	22.268	0.0855	0.0193	−0.0172	0.0020	1.1199
CP/$Al_{12}N_{12}$ (S_3)	59	0.0410	41.051	0.0695	0.0256	−0.0338	−0.0082	0.7568
	75	0.0429	42.989	0.0977	0.0314	−0.0384	−0.0069	0.8179
	85	0.0428	42.859	0.0973	0.0312	−0.0382	−0.0069	0.8179
CP/C_{12}–B_6N_6 (S_3)	46	0.0321	32.164	0.0886	0.0241	−0.0260	−0.0019	0.9249
	50	0.0818	81.844	−0.0600	0.0342	−0.0835	−0.0492	0.4102
CP/C_{12}–Al_6N_6 (S_2)	54	0.0433	43.361	0.0702	0.0270	−0.0365	−0.0095	0.7401
	72	0.0244	24.467	0.0555	0.0151	−0.0164	−0.0012	0.9213
	88	0.0441	44.173	0.0989	0.0323	−0.0399	−0.0075	0.8097
CP/B_6N_6–Al_6N_6 (S_2)	65	0.0453	45.305	0.1301	0.0382	−0.0439	−0.0056	0.8704
	77	0.0487	48.729	0.1054	0.0362	−0.0461	−0.0098	0.7858
	82	0.3229	322.97	−1.3588	0.2100	−0.7598	−0.5497	0.2764

4. Conclusions

To predict a suitable CP drug nanocarrier, we first studied the adsorption behaviour of the CP drug towards C_{24}, $B_{12}N_{12}$, $Al_{12}N_{12}$, C_{12}–B_6N_6, C_{12}–Al_6N_6, B_6N_6–Al_6N_6 nanocages and adsorption calculations of CP over $B_{12}N_{12}$, $Al_{12}N_{12}$ and B_6N_6–Al_6N_6 revealed preferable adsorption energies for drug delivery purposes both in gas and water phases. To gain a better insight into the sensitivity and reactivity of the nanocages, FMO analysis was performed, which revealed that E_L was shifted to downward values while the E_H was shifted to upward values after the adsorption of CP on the $B_{12}N_{12}$, $Al_{12}N_{12}$, and B_6N_6–Al_6N_6 nanocages. In gas and water phases, the energy gap tremendously decreased by about 43.56% and 37.77% for $B_{12}N_{12}$ and 20% and 45.67% for the B_6N_6–Al_6N_6 nanocage, respectively, which is not so appreciable (4.80% and 1.36% respectively) in case of $Al_{12}N_{12}$ after the adsorption of CP. The Hirshfeld charge analysis revealed that the charge transfer between CP and $Al_{12}N_{12}$ is not quite good enough (0.122*e* and 0.239*e* in the gas and water phases, respectively) whereas a significant amount of charge transfer was observed in the case of $B_{12}N_{12}$ (0.254*e* and 0.355*e* in gas and water phases, correspondingly) and B_6N_6–Al_6N_6 (0.312*e* in the gas phase and 0.839*e* in the water phase). The global descriptors also project that $B_{12}N_{12}$ nanocages exhibit high sensitivity and reactivity since the decrement of the global hardness and increment of global softness and the electrophilicity index of $B_{12}N_{12}$ is more preferable than that of $Al_{12}N_{12}$ after adsorption. We investigated the variations of quantum molecular descriptors of the heteronanocages as well as observed the propensity of the downfall of global hardness and rise of global softness and electrophilicity index in the case of B_6N_6–Al_6N_6. Dipole moment, work function, and COSMO surface analysis are also in favour of B_6N_6–Al_6N_6 being a potent candidate in CP drug delivery. Therefore, adsorption energy, electronic properties, Hirshfeld analysis, and quantum molecular descriptors indicate that $B_{12}N_{12}$ and B6N6–Al_6N_6 are promising candidates for targeted delivery of CP.

Conflicts of interest

The authors declare that they have no known competing financial interests or personal relationships that could have appeared to influence the work reported in this paper.

References

1 R. a Alderden, M. D. Hall and T. W. Hambley, *J. Chem. Educ.*, 2006, **83**, 728–734.
2 J. Topps and R. C. Elliott, *Nature*, 1965, **205**, 498–499.
3 B. Rosenberg, E. Renshaw, L. Vancamp, J. Hartwick and J. Drobnik, *J. Bacteriol.*, 1967, **93**, 716–721.
4 R. S. Go and A. A. Adjei, *J. Clin. Oncol.*, 1999, **17**, 409–422.
5 M. Perveen, S. Nazir, A. W. Arshad, M. I. Khan, M. Shamim, K. Ayub, M. A. Khan and J. Iqbal, *Biophys. Chem.*, 2020, **267**, 106461.
6 F. ud Din, W. A. Aman, I. Ullah, O. S. Qureshi, O. Mustapha, S. Shafique and A. Zeb, *Int. J. Nanomed.*, 2017, **12**, 7291–7309.
7 J. H. Moon, J. W. Moxley, P. Zhang and H. Cui, *Future Med. Chem.*, 2015, **7**, 1503–1510.
8 L. Qi, Q. Luo, Y. Zhang, F. Jia, Y. Zhao and F. Wang, *Chem. Res. Toxicol.*, 2019, **32**, 1469–1486.
9 N. Pontillo, F. Pane, L. Messori, A. Amoresano and A. Merlino, *Chem. Commun.*, 2016, **52**, 4136–4139.
10 A. A. Piya, S. U. D. Shamim, M. N. Uddin, K. N. Munny, A. Alam, M. K. Hossain and F. Ahmed, *Comput. Theor. Chem.*, 2021, **1200**, 113241.
11 N. Wazzan, K. A. Soliman and W. S. A. Halim, *J. Mol. Model.*, 2019, **25**, 1–19.
12 Q. Luo and W. Gu, *Mol. Phys.*, 2020, **118**, 1–7.
13 T. C. Johnstone, K. Suntharalingam and S. J. Lippard, *Chem. Rev.*, 2016, **116**, 3436–3486.
14 R. Singh and J. W. Lillard, *Exp. Mol. Pathol.*, 2009, **86**, 215–223.
15 A. N. Al-Kenani, *Open J. Discrete Math.*, 2012, **02**, 1–4.
16 B. T. Tomić, C. S. Abraham, S. Pelemiš, S. J. Armaković and S. Armaković, *Phys. Chem. Chem. Phys.*, 2019, **21**, 23329–23337.

17 A. Hosseinian, E. Vessally, S. Yahyaei, L. Edjlali and A. Bekhradnia, *J. Cluster Sci.*, 2017, **28**, 2681–2692.
18 P. R. C. Kent, M. D. Towler, R. J. Needs and G. Rajagopal, *Phys. Rev. B: Condens. Matter Mater. Phys.*, 2000, **62**, 15394–15397.
19 M. B. Javan, A. Soltani, Z. Azmoodeh, N. Abdolahi and N. Gholami, *RSC Adv.*, 2016, **6**, 104513–104521.
20 A. Soltani, A. Sousaraei, M. Bezi Javan, M. Eskandari and H. Balakheyli, *New J. Chem.*, 2016, **40**, 7018–7026.
21 F. Azarakhshi, S. Shahab, S. Kaviani and M. Sheikhi, *Lett. Org. Chem.*, 2020, **18**, 640–655.
22 R. Padash, M. R. Esfahani and A. S. Rad, *J. Biomol. Struct. Dyn.*, 2020, 1–11.
23 A. Hosseinian, A. Bekhradnia, E. Vessally, L. Edjlali and M. D. Esrafili, *Comput. Theor. Chem.*, 2017, **1115**, 114–118.
24 M. K. Hazrati, Z. Bagheri and A. Bodaghi, *Phys. E*, 2017, **89**, 72–76.
25 X. F. Fan, Z. Zhu, Z. X. Shen and J. L. Kuo, *J. Phys. Chem. C*, 2008, **112**, 15691–15696.
26 İ. Muz, F. Göktaş and M. Kurban, *Phys. E*, 2022, **135**, 114950.
27 D. Paul, J. Deb, B. Bhattacharya and U. Sarkar, *J. Mol. Model.*, 2018, **24**, 1–13.
28 B. Delley, *J. Chem. Phys.*, 2000, **113**, 7756–7764.
29 B. Delley, *J. Chem. Phys.*, 1990, **92**, 508–517.
30 J. P. Perdew, K. Burke and M. Ernzerhof, *Phys. Rev. Lett.*, 1996, **77**, 3865–3868.
31 J. P. Perdew, J. A. Chevary, S. H. Vosko, K. A. Jackson, M. R. Pederson, D. J. Singh and C. Fiolhais, *Phys. Rev. B*, 1993, **48**, 4978.
32 N. A. Benedek, I. K. Snook, K. Latham and I. Yarovsky, *J. Chem. Phys.*, 2005, **122**, 144102.
33 S. Grimme, *J. Comput. Chem.*, 2006, **27**, 1787–1799.
34 F. Ortmann, F. Bechstedt and W. G. Schmidt, *Phys. Rev. B: Condens. Matter Mater. Phys.*, 2006, **73**, 205101.
35 Y. Inada and H. Orita, *J. Comput. Chem.*, 2007, **29**, 225–232.
36 X. Chen, J. Jiang, Q. Liang, R. Meng, C. Tan, Q. Yang and X. Sun, *J. Mater. Chem. C*, 2016, **4**, 7004–7012.
37 S. U. Daula Shamim, M. K. Hossain, S. M. Hasan, A. Hossain and F. Ahmed, *Mol. Simul.*, 2020, **46**, 1135–1145.
38 A. S. Rad, S. S. Shabestari, S. A. Jafari, M. R. Zardoost and A. Mirabi, *Mol. Phys.*, 2016, **114**, 1756–1762.
39 P. K. Chattaraj and R. G. Parr, in *Chemical Hardness*, 2006, pp. 11–25.
40 W. R. Wadt and P. J. Hay, *J. Chem. Phys.*, 1985, **82**, 284–298.
41 R. G. Pearson, *Inorg. Chem.*, 1988, **27**, 734–740.
42 F. L. Hirshfeld, *Theor. Chim. Acta*, 1977, **44**, 129–138.
43 S. N. Ema, M. A. Khaleque, A. Ghosh, A. A. Piya, U. Habiba and S. U. D. Shamim, *RSC Adv.*, 2021, **11**, 36866–36883.
44 T. Ahmed, M. Aminur Rahman, R. Islam, A. Akter Piya and S. Ud Daula Shamim, *Comput. Theor. Chem.*, 2022, **1214**, 113797.
45 S. U. D. Shamim, M. H. Miah, M. R. Hossain, M. M. Hasan, M. K. Hossain, M. A. Hossain and F. Ahmed, *Phys. E*, 2022, **136**, 115027.
46 Y. F. Chang, J. P. Zhang, H. Sun, B. Hong, Z. An and R. S. Wang, *Int. J. Quantum Chem.*, 2005, **105**, 142–147.
47 K. A. Soliman and S. A. Aal, *Diamond Relat. Mater.*, 2021, **117**, 108458.
48 N. Kosar, H. Tahir, K. Ayub and T. Mahmood, *J. Mol. Graphics Modell.*, 2021, **105**, 107867.
49 T. Oku, A. Nishiwaki and I. Narita, in *Science and Technology of Advanced Materials*, 2004, vol. 5, pp. 635–638.
50 M. Rakib Hossain, M. Mehade Hasan, S. Ud Daula Shamim, T. Ferdous, M. Abul Hossain and F. Ahmed, *Comput. Theor. Chem.*, 2021, **1197**, 113156.
51 G. Xiuying, G. Fengsheng, T. Yamaguchi, H. Kan and M. Kumagawa, *Cryst. Res. Technol.*, 1992, **27**, 1087–1096.
52 I. Georgieva, N. Trendafilova, N. Dodoff and D. Kovacheva, *Spectrochim. Acta, Part A*, 2017, **176**, 58–66.
53 A. Shokuhi Rad, S. Alijantabar Aghouzi, N. Motaghedi, S. Maleki and M. Peyravi, *Mol. Simul.*, 2016, **42**, 1519–1527.
54 J. Mawwa, S. U. D. Shamim, S. Khanom, M. K. Hossain and F. Ahmed, *RSC Adv.*, 2021, **11**, 32810–32823.
55 A. Soltani, E. Tazikeh-Lemeski and M. B. Javan, *J. Mol. Liq.*, 2020, **297**, 111894.
56 H. Zhu, C. Zhao, Q. Cai, X. Fu and F. R. Sheykhahmad, *Inorg. Chem. Commun.*, 2020, **114**, 107808.
57 S. Onsori and E. Alipour, *J. Mol. Graphics Modell.*, 2018, **79**, 223–229.
58 X. F. Fan, Z. Zhu, Z. X. Shen and J. L. Kuo, *J. Phys. Chem. C*, 2008, **112**, 15691–15696.
59 D. Paul, J. Deb, B. Bhattacharya and U. Sarkar, *J. Mol. Model.*, 2018, **24**, 1–13.
60 M. R. Hossain, M. M. Hasan, N. E. Ashrafi, H. Rahman, M. S. Rahman, F. Ahmed, T. Ferdous and M. A. Hossain, *Phys. E*, 2021, **126**, 114483.
61 S. U. D. Shamim, T. Hussain, M. R. Hossian, M. K. Hossain, F. Ahmed, T. Ferdous and M. A. Hossain, *J. Mol. Model.*, 2020, **26**, 1–17.
62 M. Shahabi and H. Raissi, *J. Biomol. Struct. Dyn.*, 2018, **36**, 2517–2529.
63 S. U. D. Shamim, D. Roy, S. Alam, A. A. Piya, M. S. Rahman, M. K. Hossain and F. Ahmed, *Appl. Surf. Sci.*, 2022, **596**, 153603.
64 M. G. Campbell and M. Dincă, *Sensors*, 2017, **17**, 1–11.
65 F. Li, X. Gao, R. Wang, T. Zhang and G. Lu, *Sens. Actuators, B*, 2017, **248**, 812–819.
66 S. D. O. Richardson, *Phys. Rev.*, 1924, **23**, 153.
67 R. F. Matta and C. F. Bader, *Proteins: Struct., Funct., Bioinf.*, 2002, **48**, 519–538.
68 I. Rozas, I. Alkorta and J. Elguero, *J. Am. Chem. Soc.*, 2000, **122**, 11154–11161.